The International Journal Of Engineering And Science (IJES)
||Volume||2 ||Issue|| 3 ||Pages|| 34-40 ||2013||
ISSN(e): 2319 – 1813 ISSN(p)**:** 2319 – 1805

Silicon Solar Microcells

[1,]S.Sumera Fatima, [2,]Deepthi.P, [3,]Kendagannaswamy
[1,2,3,]Mtech1[st]semstudents,AssisstantProfessor,Dept of IT(BMSP&I),
R V College,Banglore

----------**Abstract**----------
In this paper we describe modules that use large-scale arrays of silicon solar microcells created from bulk wafers and integrated in diverse spatial layouts on foreign substrates by transfer printing. The resulting devices can offer useful features, including high degrees of mechanical flexibility, user-definable transparency and ultrathin-form-factor microconcentrator designs. Detailed studies of the processes for creating and manipulating such microcells, together with theoretical and experimental investigations of the electrical, mechanical and optical characteristics of several types of module that incorporate them, illuminate the key aspects.

Key Words:μ-cells,μ-bar,SEM,

Date Of Submission: 4 .March, 2013 Date Of Publication: 25 March 2013

I. INTRODUCTION

The practical means to create and manipulate monocrystalline Si solar cells that are much thinner (down to _100 nm, or limited only by junction depth) and smaller (down to a few micrometres) than those possible with other process technologies.The small sizes of the cells and the room-temperature schemes for integrating them into modules enable the use of thin, lightweight flexible substrates for ease of transport and installation.The ability to define the spacings between cells in sparse arrays provides a route to modules with engineered levels of transparency, there by creating opportunities for use in windows and other locations that benefit from this feature. Alternatively, such layouts of cells can be combined with moulded micro-optic concentrators to increase the power output and provide an unusual appearance with some aesthetic appeal. Such design attributes, together with the thin geometries of the microcells (μ-cells), are also advantageousbecause they can optimally balance optical absorption and carrierseparation/collection efficiency with materials usage and purityrequirements to reduce system cost. The following describes theseaspects, beginning with the materials and integration strategies,and following with characteristics of the μ-cells and variousdifferent modules that incorporate them.

Theprocess, which builds on our recent work in single-crystallinesilicon for flexible electronics22–24, begins with delineation of thelateral dimensions of microbar (μ-bar) structures on a Sip-type, boron-doped, single-crystalline wafer with aresistivity of 10–20 □cm, which we refer to as the source wafer, by etching through a patterned mask. Aligning the lengths of these structures perpendicular to the Sih1¯10i direction of the wafer places their long axes along the preferential etching plane for anisotropic, undercut etching with KOH. Regions of narrowed widths at the ends of the μ-bars serve as anchors to retaintheir lithographically defined positions throughout the processing.Maintaining sharp-angled corners at the positions of these anchors leads to stress focusing for controlled fracture25 in the printingstep, as described below. After etching, selective-area diffusionof boron (p+) and phosphorus (n+) from solid doping sourcesthrough patterned diffusion barriers of SiO2 creates rectifying pn junctions and top contacts. Deposition of etch masks (SiO2–Si3N4,Cr–Au) on the top surfaces and sidewalls of the μ-bars followed by KOH etching releases them from the source wafer everywhere except at the positions of the anchors. Boron doping at the exposed bottom surfaces of the μ-bars, again using a solid doping source,creates a back-surface field to yield fully functional Si solar μ-cells. Figure 1c providesscanning electron micrograph of arepresentative array of μ-cells on a source wafer where the bars havelengths (*L*), widths (*W*) and thicknesses (*t*) of 1.55 mm, 50 μmand15 μm.

Figure 1a schematically illustrates the steps for fabricatingultrathin, monocrystalline silicon solar µ-cells along with methodsfor integrating them into interconnected modules (Fig. 1b).

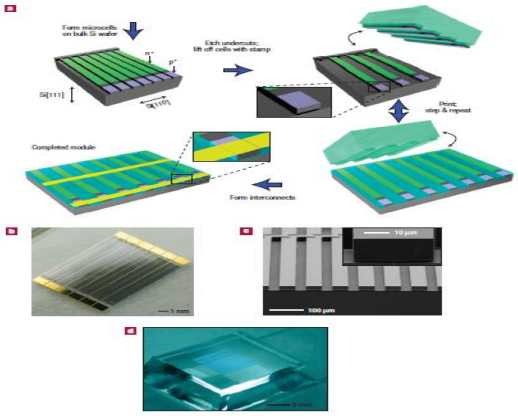

Figure 1Schematic illustrations, scanning electron microscopy (SEM) image and optical images of key steps in the fabrication of monocrystalline silicon photovoltaic modules that incorporate arrays of microscale solar cells (µ-cells). a, Schematic illustration of steps for fabricating ultrathin µ-cells from a bulk wafer,printing them onto a target substrate and forming electrical interconnections to complete a module. **b**, Optical image of a completed module consisting of printed µ-cellarrays.**c**, SEM image of an array of µ-cells on a source wafer,ready for printing, after doping and KOH undercut. The inset shows a magnified cross-sectional SEM image of a typical µ-cell, with thickness of _20 µm. **d**, Optical image ofan array of µ-cells on a flat elastomeric poly(dimethylsiloxane) immediately after retrieval from a source wafer.

Figure 2a schematically illustrates the layout of a representative µ-cell design, highlighting the details of the doping profiles.

An individual cell (L = 1.55mm) consists of phosphorus-doped (Ln+ = 1.4 mm), boron-doped (Lp+ = 0.1mm) and un-doped (Lp = 0.05mm) regions, respectively. The thicknesses, t, can be selected by suitable processing to lie between tens of micrometres and hundreds of nanometres. The boron-doped region on the top of the cell connects to the back-surface field on the bottom through doping on the sidewalls, in a manner that enablesaccess to both emitter (n+) and base (p+) contacts on the top surface. This configuration greatly simplifies the process of electrical interconnection to form modules, by providing both contacts on the same side of the device. Surface doping concentrations of n+ (phosphorus), p+ (boron) and back-surface field (boron) regions are _1.2×1020 cm−3, _1.8×1020 cm−3 and _5.8×1019 cm−3, respectively, as measured by secondary-ion massspectrometry . To fabricate interconnects with high yields, we identified two convenient means for planarizing the relief associated with the µ-cells and for ensuringelectrical isolation of the emitter and the base. The first uses a photocurable polymer as both an adhesive and planarization.medium, as described in the context of Fig.1.

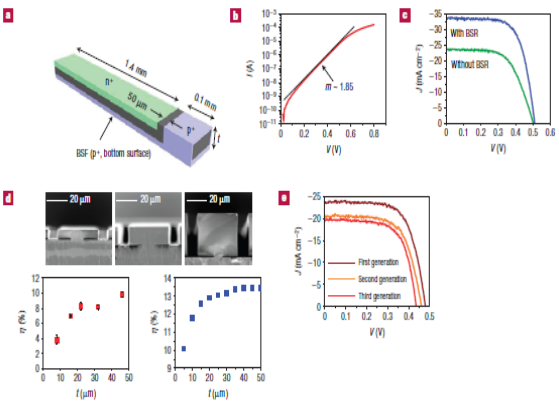

Figure 2Doping layout and performance characteristics of individual µ-cells.a, Schematic illustration of a µ-cell, showing the dimensions and the doping profiles.**b**, Semilog plot of the forward-bias dark-current (I)–voltage (V) characteristics of an individual µ-cell. The linear fit corresponds to a diode ideality factor (m) of _1.85.**c**, Representative current-density (J) and voltage (V) data from an individual µ-cell with thickness of _15 µm

under Air Mass 1.5 (AM 1.5) illumination of 1,000Wm2,with and without a white diffuse backside reflector (BSR). **d**, SEM images, experimental efficiency data (with a metallic BSR) and PC-1D software modelling resultscorresponding to studies of the scaling properties with thicknesses between 8 and 45 μm. **e**, Light J–V curves of individual μ-cells corresponding to the first, secondand third generations from a single source wafer, with thickness of 15 μm.

Medium, as described in the context of Fig. 1 (see Supplementary Information, Fig. S4), such that a single step accomplishes both printing and planarization. Here, arrays of μ-cells on the stamp press down into a liquid, photocurable polymer (NOA61) coated on the receiving substrate. The polymer fills the empty space between the μ-cells by capillary action. Curing by ultraviolet exposure through the transparent stamp and then removing the stamp completes the process. The flat surface of the stamp coincides precisely with the top surfaces of the μ-cells, to define the planarized surface of the module. Another approach (see Supplementary Information, Fig. S5), which is better suited to a step-and-repeat process, involves printing μ-cells on a substrate that is coated with a layer (_10 μm thick) of cured PDMS (Dow Corning) as a soft, elastomeric adhesive. Covering the printed μ-cells with thin layers of SiO2 (_150nm thick) and NOA61 (_30 μm thick), pressing a flat piece of PDMS on top of the structure and then ultraviolet curing through the stamp accomplishes planarization with a tolerance (less than 1 μm) similar to that achieved in the first approach. In this second method, a short oxygen reactive-ion etching step is often needed to remove the thin, residual layer of NOA61 that tends to coat partially the top surfaces of the μ-cells. In both approaches, the shallow junction depth (_0.3 μm) creates challenging demands on the extent of planarization.

Extending the photodistance of 1/3 of the μ-cell thickness, as illustrated in Fig. 2a, relaxes the requirements on planarization. Direct ink writing and other approaches that formconformal electrodes provide further benefits in this sense. *I–V* measurements of individual μ-cells and completed modules were made in the dark and in a simulated AM 1.5 illumination condition of 1,000Wm−2 at room temperature. Figure 2b shows a representative dark *I–V* curve recorded from an individual μ-cell under forward bias, indicating a diode ideality factor (*m*) of _1.85 at room temperature. Figure 2c shows *I–V* curves from typical μ-cells with and without a backside reflector (BSR) under AM 1.5 illumination, evaluated without metal contacts or antireflection coatings.Without a BSR, this μ-cell,which has *t* _ 15 μm, shows a short-circuit current density, *J*sc, of 23.6mAcm−2, an open-circuit voltage, *V*oc, of 503mV, a fill factor of 0.61 and an overall solar-energy conversion efficiency of 7.2%, where the calculations relied on the spatial dimensions of the μ-cells rather than the surface area of the p–n junction. We also do not explicitly account for contributions from light incident on the edges of the cells. The device-to-device variations in properties of the μ-cells of 15–20 μm thickness without BSR are typically in the range of 6–8% (10–13% with BSR) for _ and 450–510mV for *V*oc. In this ultrathin regime, the absorption length of monocrystalline Si for near-infrared and visible wavelengths is greater than or comparable to *t* (refs 29,30).

As a result, the efficiency can be improved significantly by adding structures for light-trapping and/or a BSR. The top curve in Fig. 2c shows the effects of a diffuse white BSR, where *J*sc and _ increase to 33.6mAcm−2 (_42% increase) and 11.6% (61% increase), respectively. The *J*sc value without a BSR in Fig. 2c is close to the theoretical maximum of _26mAcm−2 that would be expected on the basis of the solar spectrum and absorption coefficient of Si, suggesting that the surface and contact recombination in the device was modest under short-circuit conditions. With the BSR the gain in *J*sc to 33.6mAcm−2 is consistent with a 56 μmequivalentthickness (on the basis of the required thickness for sufficient absorption of light). The much higher optical path length shows that the BSR is working well. To further examine the dependence of performance on thickness, we tested μ-cells with *t* between _8 and _45 μm and compared the measurements with numerical simulation of conventional cells using PC-1D software31, in vertical-type (n+–p–p+) configurations (see Supplementary Information, Fig. S6 and Table S1). Figure 2d shows the results, which indicate sharp increases in efficiency with thickness up to _15 μm, followedby a gradual saturation from 20 to 30 μm to a plateau above40 μm. Increases in efficiency with *t* are due mainly to increased absorption associated with the longer optical path lengths. For *t* above _40 μm, however, the total absorption does not increase significantly, though the bulk recombination of minority carriers does. Although there are some quantitative differences between measurement and theory owing to non-ideal features of the μ-cells (such as edge surface recombination due to un-passivated surfaces), the qualitative trends are consistent. These observations highlight the value of ultrathin (that is, less than 40 μm) cell designs, both in optimizing materials usage and in minimizing sensitivity to impurities that can lead to trapping of carriers. As described previously, multiple generations of such ultrathin cells can be created from a single wafer. Figure 2e shows results from first-, second- and third-generation devices produced from a single source wafer in conventional vertical-type (n+–p–p+) cell configurations. Only moderate changes, comparable to typical cell-to-cell variations in properties, are observed. Improved doping profiles, ohmic contacts, antireflection coatings, surface texturization, light trapping

structures, surface passivation layers and other advanced designs for monocrystalline Si cells can all be implemented within the schemes described here; each has thepotential to provide improvements over the performance indicated in Fig. 2. The μ-cell designs and printing techniques enable new opportunities at the module level, with performance consistent with that of the individual cells. For example, the sequence in Fig. 1 separates high-temperature processing steps fromthe module substrate. As a result, integration of μ-cells on rollable, plastic sheets, for ease of transport and installation, is possible. High levels of bendability can be achieved by exploiting optimized mechanical designs.

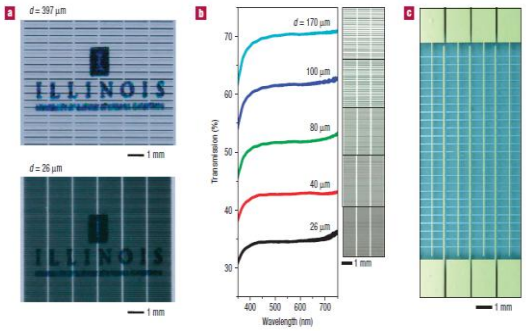

Fig. 3Optical images and transmission spectra of printed,semitransparentμ-cell arrays and interconnected modules. a.Optical images of printed μ-cell arrays on coated polyethylene terephthalate substrates. b.Transmission spectra recorded at normal incidence through printed semitransparent μ-cell arrays. C.Optical image of aninterconnected semitransparent module.

Figure 3a shows printed text and logos viewed through arrays ofμ-cells with high and low areal coverages, to demonstrate the effect.Automated printer enable programmable selection of coverages and, therefore, levelsof transparency, for any given arrangement of μ-cells on the sourcewafer. Figure 3b shows normal-incidence transmission spectra andoptical micrographs for cases of cell spacings ranging from 170to 26 μm (areal coverages from 20% to 60%), corresponding tolevels of transparency from _70% to _35%, all generated fromarrays of μ-cells on a single source substrate. The transmittance ineach case is constant throughout the visible range, and increasesapproximately linearly with areal coverage, as expected. Figure 3cprovides an image of a completed module, with interconnects,consisting of μ-cells at a spacing of 397 μm.For cells in such layouts, concentrator photovoltaicdesigns that use integrated micro-optic focusing elements forultrathin-form-factor microconcentratorphotovolt systems can improve the module's output power. Here, wedemonstrate this possibility with moulded arrays of cylindricallenses, for possible implementation with a single-axis tracker. These devices use arrays of μ-cells with spacings (_397 μm) thatmatch the layouts of low-cost, commercially available lenticularlens arrays (Edmund Optics), from which we could form replicasby soft lithographic moulding of a composite silicone-based epoxy resin that was thermally matched to the photovoltaic moduleby filling with silica nanoparticles.

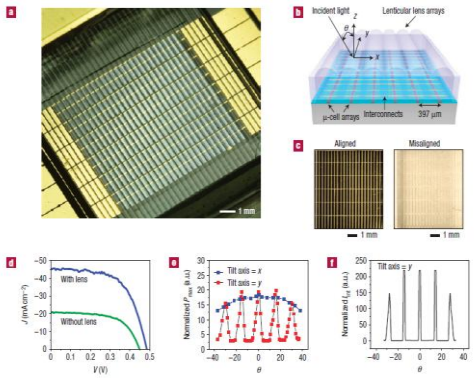

Fig. 4Optical images, schematic illustration and performance characteristics of μ-CPV modules.**a**, Optical image of a μ-CPV module that combines mouldedlenticular lens arrays and printed μ-cells.**b**, Schematicillustration of this type of device.**c**, Optical images of lenticular lens arrays aligned (left) and misaligned (right) to arrays of printed μ-cells,d,J–V curves of this μ-CPV module with and without the lenticular concentrator optics under AM 1.5 illumination.**e**, Normalized output power. **f**, Normalized computed intensity.

Figure 4a,bshows an optical image and a schematic illustration of such aμ-CPV device. Figure 5c presents images corresponding to thecases when the lens arrays are aligned and misaligned to the μ-cells.In the aligned state, the module seems to incorporate silicon at a nearly full areal coverage. .When misaligned, the ystemassumes thecolour of the module substrate, and the silicon is invisible. The *I–V*characteristics of a module with and without aligned lens arrays,under AM 1.5 illumination, are shown in Fig. 4d. The maximumoutput power with the lenses is _2.5 times larger than that withoutthe lenses. This ratio is somewhat smaller than the expectation onthe basis of simple estimates ,owing partly to the relatively large size of the light source in thesolar simulator (91192-1000W, Oriel) and its close proximity tothe module. These features result in a degree of collimation thatis both non-ideal and substantially less than that of sunlight.However, the small area and ultrathin microdesigns presentedhere can in principle lead to consumption of less silicon materialthan conventional and related microspherical silicon concentratormodules9. Owing to the cylindrical geometry of the lenses and thebar shapes of the μ-cells, decreases in output power associated withangular tilting about the *x*-axis are minimal, as illustrated in Fig. 4e.Rotations about the *y*-axis cause dramatic changes, consistent withthe nature of the optics and the images shown in Fig. 4c. Theperiodicity observed in this case results from focusing of light onμ-cells from neighbouring sets of lenses. The angular positions andrelative values of the first, second and third peaks match well withsimulated data from numerical ray-tracing calculations (Fig. 4f).

The types of module reported here may create new possibilities for monocrystalline silicon photovoltaics, particularlyin applications that benefit from thin, lightweight construction,mechanical flexibility, semitransparency or the unusual opticalproperties of the μ-CPV designs. In most cases, we chose materialsthat have the potential for long lifetime and high reliability. The procedures themselves are compatible with substrates,encapsulation, adhesive and optical materials used in existingphotovoltaic systems. Similarly, as noted previously, advancedmonocrystalline silicon cell designs and enhancement techniquescan also be incorporated for improved performance. Although thefocus of the strategies presented here is on module capabilities anddesigns, rather than cost or performance, a notable feature of theseapproaches is that the ultrathin cell geometries and, for μ-CPV andsemitransparent designs, the sparse coverages represent efficientways to use silicon. The former aspect can also relax requirementson the purity of the silicon. An obvious consequence of theseaspects is the potential to reduce the silicon component of themodule cost. Such reductions are balanced, however, by increasedprocessing costs associated with creating and interconnecting theμ-cells. Low-cost printing, doping and etching techniques suitablefor high-performance μ-cell and module fabrication, together withother means to reduce cost or increase performance, are, therefore,
important areas for further work.

II. METHODS

2.1 FABRICATING MICROCELLS

The fabrication process began with a p-type (111) Si wafer thatwas coated with a layer of SiO2 (600 nm) formed by plasma-enhancedchemical vapour deposition (PlasmaTherm SLR) at 250 _C. Spin casting,exposing (365nm light, through a Karl Suss MJB mask aligner) and developinga layer of photoresist formed a pattern that defined the lateral dimensions and layouts of the μ-cells,in rectangular geometries (that is, μ-bars). The SiO2 not protected by theresist was removed with buffered oxide etchant (6:1, Transene). Inductivelycoupled plasma reactive-ion etching (STS)23,24 formed trench structures withtypical depths of 15–20 μm in the regions of exposed silicon.The photoresistand remaining SiO2 were then removed with acetone and hydrofluoric acid(HF, Fisher, 49% concentration), respectively. Selective area doping of topcontacts was conducted using solid-state sources of boron and phosphorus at 1,000 _C under N2atmosphere for 30 min (boron) and 10 min (phosphorus). A layer of SiO2(900 nm) deposited by plasma-enhanced chemical vapour deposition at 250 _Cand patterned by photolithography and etching in bufferedoxide etchant served as a doping mask. The doped wafer was then cleanedand coated with SiO2 (100 nm) and Si3N4 (500 nm) by plasma-enhancedchemical vapour deposition at 250 _C, and subsequently with Cr (80 A°)and Au (800 A°) via directional deposition in an electron-beam evaporator at an angle of ±30_ with respect to the wafer surface.Reactive-ion etching using CHF3–O2 and SF6 exposedregions of Si at the bottoms of the trenches formed by inductively coupledplasma reactive-ion etching. Immersion in KOH at100 _C for _30 min initiated anisotropic undercut etching at these locationsto define the bottom surfaces of the μ-cells with overall yields of over99%. After removing Au and Cr with commercial etchants ,these bottom surfaces were doped with boron again using the solid-statedoping source at 1,000 _C for 5 min. Cleaning of the resulting sample inPiranha solution and HF completedthe process.

2.2 FABRICATING ELASTOMERIC STAMPS

Simple, flat stamps for by-hand printing were prepared by curing a PDMSprepolymer and cross-linking agent mixedat 10:1 by volume at 75 _C for 2 h. Forming composite stamps suitable for usein our automated printer system involved several steps (see SupplementaryInformation, Fig. S3). First, the template that defined the geometry of relief onthe stamp was prepared on a Si wafer (4 inch diameter) by optical lithographyusing a negative-tone photoresistand a developer . This substrate was thenexposed to a vapour of -1-tricholorosilane for 3 h at room temperature. A10:1 PDMS prepolymer mixture was poured onto the substrate, to a thicknessof 100–200 μm, and then partially cured at 75 _C for 30 min. A thin glass disc was placed ontop, to form a backing layer capable of reducing in-plane deformations duringprinting. As a final step, another layer of 10:1 PDMS prepolymer mixture waspoured on top. The entire composite stamp was heated at 75 for 2 h, tocomplete the curing.

2.2 TRANSFER PRINTING MICROCELLS

Transfer printing used a custom-built, automated machine consisting ofmotion-controlled stages with 1 μm resolution and an optical microscopevision system with a zoom range of 4× to 26×. Vacuum chucks mount onmanually controlled rotational stages with 6 arc seconds sensitivity to supportthe processed wafers and the target substrates and to align them with each otherand the relief features of the stamp. These chucks rest on a computer-controlledstage capable of 8 inches of motion in the *X* and *Y* directions. A PDMScomposite stamp bolts into a vertical printhead assembly that can move in thevertical (*Z*) direction up to 2 inches. The stamp mount has a square, 3 inchaperture enabling an optical microscope vision system to image through thetransparent composite stamp onto the stages below. The steps for printing areas follows.To ensure high yields, it is critical that all components of the system areproperly aligned. The tilt of the PDMS composite stamp relative to the sourcewafer and target substrate was manually adjusted, with 20 arc seconds ofsensitivity, using the vision system for guidance. The μ-cells on the source waferwere aligned to the corresponding relief features on the composite stamp rotational stages on the *XY* stage. A two-point calibration must be carried outon the source wafer, target substrate and cleaning substrate (six points in total)to account for tilt in the *Y* direction as well as misalignment of the *XY* motionaxes relative to the orientation of the stamp.

2.3 PLANARIZING MICROCELLS

In planarization method 1, a precleaned substrate was exposed to ultraviolet-induced ozone for 10 min and thenspin-coated with an ultraviolet-curable polymer . Retrieved μ-cells on a flat PDMS stamp were placed against this substrateand then the entire system was exposed to an ultraviolet source for 30 min tocure the NOA. The PDMS stamp was then slowly peeled from the substrate,leaving planarized μ-cells in a NOA matrix.ln planarization method 2, after printing arrays of μ-cells on a substratewith a thin PDMS coating, SiO2 (150 nm) was deposited by electron-beamevaporation . Spin-coating a layer of NOA61 (_30 μm) andthen contacting a bare, flat PDMS element caused the NOA to flow to conformto and planarized the relief presented by the μ-cells. Curing the NOA by exposureto ultraviolet light followed by removal of the stamp and, sometimes, a briefexposure of the substrate to an oxygen reactive-ion etch completed the process.

2.4 OPTICS SIMULATION

The calculation was carried out with a commercial ray-tracing package . We assumed that the rays of light were incident at oneangle and had a wavelength of 550 nm, that the lens array was infinite andthat Fresnel reflections were negligible. The curved surface of the lens arraywas profiled experimentally and fitted to a parabola; the width of each lenswas _0.4mm and its centre thickness was _2.2 mm. The lens material wastaken to be BK7 glass (for the purposes of this calculation). The lens arraywas positioned 0.1mm from the top surface of the μ-cells, whose width was0.05 mm. The integrated top surface intensity is an imperfect predictor of thepower incident and absorbed by the μ-cells. However, the periodicity of theμ-cell response with incident angle is captured.

III. CONCLUSION AND FUTURESCOPE

Here,we describemodules that use large-scale arrays of silicon solar microcells created frombulk wafers and integrated in diverse spatial layouts on foreign substrates by transfer printing. The resulting devices can offer usefulfeatures, including high degrees of mechanical flexibility, user-definable transparency and ultrathin-form-factor microconcentratordesigns. Detailed studies of the processes for creating and manipulating such microcells, together with theoretical and experimentalinvestigations of the electrical, mechanical and optical characteristics of several types of module that incorporate them, illuminate then key aspects.Research in silicon photovoltaics represents a robust and diverseeffort, with foci that seek to improve performance, costand capabilities of these systems, ranging from structures forlight trapping1 to advanced doping techniques, innovativespherical, rectangular and ultrathin cell designs andadvanced manufacturing techniques. The results presented herecontribute to this progress by introducing practical means tocreate and manipulate

monocrystalline Si solar cells that aremuch thinner and smaller than thosepossible with other process technologies.

REFERENCES

[1] Biancardo, M. et al. Characterization of microspherical semi-transparent solar cells and modules. Sol.Energy**81**, 711–716 (2011).

[2]. Liu, Z. X. et al. A concentrator module of spherical Si solar cell.Sol. Energy Mater. Sol. Cells **91**,1805–1810 (2010).

[3]. Minemoto, T. &Takakura, H. Fabrication of spherical silicon crystals by dropping method and theirapplication to solar cells. Jpn. J. Appl. Phys. **46**, 4016–4020 (2009).

[4] Feng, N.-N. et al. Design of highly efficient light-trapping structures for thin-film crystalline siliconsolar cells. IEEE Trans. Electron Devices **54**, 1926–1933 (2009).

[5] Weber, K. J. et al. A novel low-cost, high-efficiency micromachined silicon solar cell.IEEE ElectronDevices Lett.**25**, 37–39 (2009).

[6]. Verlinden, P. J. et al. Sliver (R) solar cells: A new thin-crystalline silicon photovoltaic technology. Sol.Energy Mater. Sol. Cells **90**, 3422–3430 (2009).

[7] Bergmann, R. B. Crystalline Si thin-film solar cells: A review. Appl. Phys. A **69**, 187–194 (2009)

.[8]. Green, M. A. Crystalline and thin-film silicon solar cells: State of the art and future potential. Sol. Energy **74**, 181–192 (2008).

[9] Kazmerski, L. L. Solar photovoltaics R&D at the tipping point: A 2005 technology overview. J. Electron Spectrosc. Relat.Phenom.**150**, 105–135 (2008).

[10] Mack, S., Meitl, M. A., Baca, A. J., Zhu, Z. T. & Rogers, J. A. Mechanically flexible thin-film transistorsthat use ultrathin ribbons of silicon derived from bulk wafers. Appl. Phys. Lett. **88**, 213101 (2007).

[11]. Ko, H. C., Baca, A. J. & Rogers, J. A. Bulk quantities of single-crystal silicon micro-/nanoribbonsgenerated from bulk wafers. Nano Lett. **6**, 2318–2324 (2008).

[12]. Baca, A. J. et al. Printable single-crystal silicon micro/nanoscale ribbons, platelets and bars generatedfrom bulk wafers. Adv. Funct. Mater.**17**, 3051–3062 (2007).

[13]. Meitl, M. A. et al. Stress focusing for controlled fracture in microelectromechanical systems. Appl.Phys. Lett. **90**, 083110 (2007).

[14]. Meitl, M. A. et al. Transfer printing by kinetic control of adhesion to an elastomeric stamp. Nature Mater.**5**, 33–38 (2008).

[15]. Lee, K. J. et al. Large-area, selective transfer of microstructured silicon: A printing-based approach tohigh-performance thin-film transistors supported on flexible substrates. Adv. Mater. **17**, 2332–2336 (2008).

[16] Brendel, R. Review of layer transfer processes for crystalline thin-film silicon solar cells. Jpn. J. Appl.Phys.**40**, 4431–4439 (2007).

[17]. Tayanaka, H., Yamauchi, K. & Matsushita, T. Thin-film crystalline silicon solar cells obtained by separation of a porous silicon sacrificial layer. Proc. 2nd World Conf. Photovolt.Sol. Energy Conv.1272–1275 (Institute of Electrical and Electronics Engineers (IEEE), 2007).

[18]. Yamamoto, K. et al. Thin-film poly-Si solar cells on glass substrate fabricated at low temperature.Appl. Phys.A **69**, 179–185 (2007).

[19]. Shah, A. et al. Photovoltaic Specialists Conference, Conference Record of the Twenty-Sixth IEEE569–574 (2007).

[20] Clugston, D. A. &Basore, P. A. Photovoltaic Specialists Conf. 1997., Conf. Record of the Twenty-SixthIEEE207–210 (Institute of Electrical and Electronics Engineers (IEEE), 2006).

[21]. Kunnavakkam, M. V. et al. Low-cost, low-loss microlens arrays fabricated by soft-lithography replication process. Appl. Phys. Lett. **82**, 1152–1154 (2003).